ACS OMEGA

Open Access

http://pubs.acs.org/journal/acsodf

Article

Identification of a Potential Antimycobacterial Drug Sensitizer Targeting a Flavin-Independent Methylenetetrahydrofolate Reductase

Jiacong Li, Yong Nian, Jian Liu, Mingxia Yang, Yuanling Jin, Xiaoman Kang, Haodong Xu, Zhuo Shang,* and Wei Lin*

Cite This: *ACS Omega* 2023, 8, 38406−38417

Read Online

ACCESS | Metrics & More | Article Recommendations | Supporting Information

ABSTRACT: The increasing antibiotic resistance of *Mycobacterium tuberculosis* and pathogenic nontuberculosis mycobacteria highlights the urgent need for new prevention and treatment strategies. Recently, the cocrystal structure of a *Mycobacterium smegmatis* flavin-independent 5,10-methylenetetrahydrofolate reductase (*Msm*MTHFR) that binds with a reduced nicotinamide adenine dinucleotide (NADH) has been well-determined, providing a structural basis for the screening of antimycobacterial leads targeting *Msm*MTHFR, a new enzyme involved in tetrahydrofolic acid (THF) biosynthesis. In this study, we identified compound AB131 as a promising candidate that fits well into the NADH binding pocket of *Msm*MTHFR through virtual screening. We discovered that AB131 and its derivatives (**13** and **14**) can sensitize the antimycobacterial activity of the antitubercular drug *para*-aminosalicyclic acid (PAS) by 2−5-fold against various species of mycobacteria. Although the compounds themselves do not exhibit any antimycobacterial activity, the high binding affinity of AB131 with *Msm*MTHFR or Rv2172c was evaluated by microscale thermophoresis analysis. Additionally, we predicted and validated the key residues (V115, V117, P118, and R163) of *Msm*MTHFR that are involved in the interaction with AB131 by using molecular docking and mutagenesis analysis. These findings offer a potential exploitable target for developing potent and specific antimycobacterial drug sensitizers.

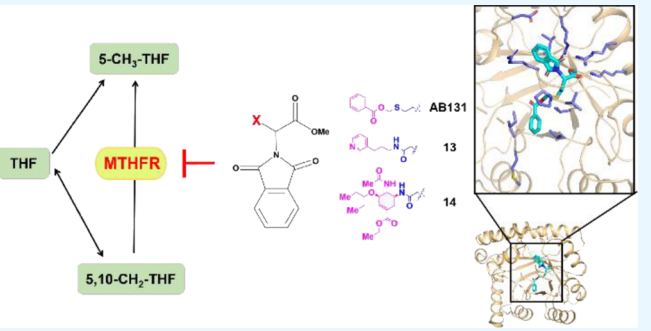

INTRODUCTION

Tuberculosis (TB) caused by *Mycobacterium tuberculosis* (*M. tuberculosis*) is a common chronic infectious disease. Although there are some new diagnostic methods of *M. tuberculosis* and antituberculosis infective drugs used for tuberculosis prevention and treatment, tuberculosis is still one of the biggest public health threats. According to the 2022 global tuberculosis report issued by the World Health Organization (WHO), it is estimated that 10.6 million people suffered from tuberculosis and more than 1.6 million people died of tuberculosis in 2021. The COVID-19 pandemic led to a 15% drop in the number of multidrug resistance (MDR) tuberculosis patients receiving treatment, a 22% drop in the number of patients receiving preventive treatment, and a 9% drop in the cost of tuberculosis prevention, diagnosis, and treatment services. The severe situation of tuberculosis infection at home and abroad calls for the research and development of better diagnostic methods, vaccines, and drugs as soon as possible. Therefore, it is urgent to study the pathogenesis and drug resistance mechanism of *M. tuberculosis* and find new drug targets against drug-resistant bacteria.

At present, the treatment of tuberculosis patients is mainly a long-term combination of rifampin, isoniazid, streptomycin, pyrazinamide, and ethambutol as antibacterial drugs. Multidrug-resistant tuberculosis patients need at least 18 to 24 months of treatment.[1−3] During the course of treatment, they need thousands of expensive tablets and daily injections, which not only brings heavy economic and psychological burden to ordinary families, but also, long-term antibiotic combined treatment is very likely to cause the emergence of drug resistance of *M. tuberculosis*. Identifying new drug targets and screening lead compounds based on these targets may be able to effectively fight against drug-resistant *M. tuberculosis*.

The folate synthesis process of bacteria has always been the focus of research and development of new anti-infective drugs.[4−6] Due to the lack of folate transporters, bacteria are not able to directly utilize folic acid in their growth environment. Therefore, they have to use *p*-aminobenzoic acid (PABA),

Received: July 14, 2023
Accepted: September 19, 2023
Published: October 4, 2023

dihydropteridine, and glutamic acid from the environment as substrates to synthesize dihydrofolate (DHF) under the catalysis of dihydropterate synthetase (DHPS). Dihydrofolate forms tetrahydrofolate (THF) under the action of dihydrofolate reductase (DHFR), and tetrahydrofolate, as a coenzyme of one carbon unit transfer enzyme, participates in the synthesis of a series of important amino acids and nucleotides such as methionine, serine, purine, and pyrimidine of bacteria.[4,5,7−10] Many current anti-infective drugs target key enzymes of bacterial folate synthesis. Sulfonamide drugs affect the synthesis of dihydrofolate through competing with PABA for dihydropterate synthetase (DHPS), thereby inhibiting bacterial growth and reproduction. The antibacterial synergist trimethoprim (TMP) selectively inhibits the enzyme activity of dihydrofolate reductase (DHFR) of bacteria, so that dihydrofolate cannot be reduced to tetrahydrofolate, thereby inhibiting the growth of bacteria.[4,7,11−15] When trimethoprim and sulfonamide drugs are used together, the bacterial folic acid synthesis is double blocked, which can not only enhance the antibacterial effect but also reduce the generation of drug resistance. In recent years, another class of antibacterial synergists targeting thymidylate synthase (TS), 5-fluorouracil (5-FU), and pemetrexed have also been successfully developed. They played a bactericidal and synergistic role by blocking the conversion of deoxyuridine to deoxythymosine catalyzed by thymidylate synthase (TS) and prevented the normal synthesis of thymine and dihydrofolate recycling by bacteria.[4,5,7] Therefore, searching for new targets from the process of folic acid synthesis may provide new ideas for the development of new anti-infective drugs.

In order to normally synthesize folic acid and thus synthesize corresponding essential amino acids and nucleotides, bacteria not only need the participation of key catalytic enzymes such as dihydrofolate synthase (DHPS), dihydrofolate reductase (DHFR), and thymidylate synthase (TS) but also an important reductase, 5,10-methylenetetrahydrofolate reductase (MTHFR); MTHFR can reduce 5,10-methylenetetrahydrofolate (N_5,N_{10}-methylene-THF; 5,10-CH_2-THF) to 5-methyltetrahydrofolate (5-methyl-THF) in the presence of nicotinamide adenine dinucleotide phosphate (NADPH)/nicotinamide adenine dinucleotide (NADH) and flavin adenine dinucleotide (FAD) catalyzed by homocysteine methyltransferase; 5-methyltetrahydrofolate can transfer methyl to homocysteine to generate methionine.[7−10,16−21] Therefore, MTHFR is critical for the transfer of one carbon unit and the synthesis of essential amino acids in organisms.

MTHFR is widely distributed in eukaryotic organisms such as mammals, nematodes, and yeast, as well as prokaryotic organisms such as *Escherichia coli* (*E. coli*) and thermophilic bacteria.[22−26] Based on the domain composition, MTHFRs can be divided into two categories: MTHFRs of eukaryotes and MTHFRs of bacteria. The MTHFR of eukaryotes contains two domains (catalytic domain and regulatory domain), while the MTHFR of prokaryotes contains only one domain (catalytic domain). MTHFRs in eukaryotic or prokaryotic organisms usually use NADH/NADPH and FAD as the source of reducing power and exist in the form of a dimer or tetramer.[10] The lack of MTHFR in humans will lead to hyperhomocysteinemia, hypomethioninemia, and a series of neurological and vascular diseases. The structure homology of the catalytic domain from MTHFR between eukaryotes and prokaryotes is high, and the amino acid sequence identity between them is about ∼50%.[10]

To identify potentially new target proteins involved in folate biosynthesis in *M. tuberculosis*, we conducted a review of the research progress in this area. Our findings suggest that the structure and catalytic mechanism of MTHFRs from *Mycobacterium smegmatis* (*M. smegmatis*), a model strain of Mycobacterium, may be highly distinctive. There were two candidate MTHFR genes in its genome: *MSMEG_ 6649* and *MSMEG_6596*. After protein expression and purification, both *MSMEG_ 6649* and *MSMEG_6596* showed the enzyme activity of MTHFRs independent of FAD,[7,10] which can directly reduce 5,10-methylenetetrahydrofolate to 5-methyltetrahydrofolate using NADH. Previous studies have speculated that the folate synthesis process of *M. tuberculosis* is similar to that of *M. smegmatis*, but only one candidate gene *MtbRv2172c* for MTHFR can be found in the genome of *M. tuberculosis*. Deng et al. found that the sensitivity of the Δ*MtbRv2172c* strain to folate synthesis antagonists such as sulfamethoxazole (SMX) and *para*-aminosalicylic acid (PAS) was significantly increased after the *MtbRv2172c* gene of *M. tuberculosis* was knocked out compared to the wild-type one,[27] suggesting that the MTHFR *Mtb*Rv2172c of *M. tuberculosis* may become a new target for the development of anti-*M. tuberculosis* infection drugs/sensitizers.

In this study, the NADH binding pocket of *Msm*MTHFR, identified in the crystal structure of *apo Msm*MTHFR and the cocrystal structure of *Msm*MTHFR with NADH (Protein Data Bank (PDB) accession numbers 7WMW and 7WMZ),[10] was targeted for molecular docking-based virtual screening to identify potential MTHFR inhibitors. Interestingly, the virtual screening identified AB131, a compound that showed a synergistically antimycobacterial effect when coadministered with PAS. Thus, our results offer a novel target for discovering improved inhibitors for folate metabolism in mycobacteria.

RESULTS AND DISCUSSION

Molecular Docking-Based Virtual Screening. As the NADH binding pocket of *Msm*MTHFR (MSMEG_6649) has been clearly defined in our recent report for the cocrystal structure of *Msm*MTHFR-NADH,[10] we hypothesized that this pocket may serve as a new target for the discovery and design of antimycobacterial drugs. To achieve this goal, a combination of virtual screening tools including the Glide module from Schrodinger Maestro 2019 and AutoDock Vina was employed to screen 202,294 chemical structures. Eventually, 35 energy-favorable candidate structures were prioritized in view of their structure similarities to NADH, the native substrate of *Msm*MTHFR (Figure S1). Next, the antimycobacterial activity of these candidate compounds was evaluated against *M. smegmatis* MC^2 155. Unfortunately, none of the candidate compounds showed antimycobacterial activities even when the compound concentration was increased to 64 μg/mL.

AB131 Is a Strong Inhibitor of MSMEG_6649 and Rv2172c. Recently, Deng et al. reported that Rv2172c is a key enzyme for folate metabolism that controls the growth of *M. tuberculosis*. Furthermore, the knockout of Rv2172c, a homologue of MSMEG_6649, resulted in an increased susceptibility of *M. tuberculosis* to *para*-aminosalicylic acid (PAS), an antibiotic primarily used to treat tuberculosis (Yu et al.). These findings inspired us to investigate the potential combination inhibitory effect of PAS or other antibacterial drugs targeting the folate pathway, such as SMX or TMP and the candidate compounds on *M. smegmatis* MC^2 155. Intriguingly, we discovered that the use of a combination of

https://doi.org/10.1021/acsomega.3c05021
ACS Omega 2023, 8, 38406−38417

Table 1. Antimycobacterial Activity of AB131 and Its Derivatives Alone or Combined with Current TB Drug PAS against Wild-Type *M. smegmatis* MC^2 155, Wild-Type *M. tuberculosis* H37Rv, Wild-Type *Mycobacterium bovis* (*M. bovis*) BCG-Pasteur, and Wild-Type *Mycobacterium marinum* (*M. marinum*) BAA-535[a]

	MIC (μg/mL)															
	drug alone				drug in combination						FICI					
mycobacterial strains	PAS	AB131	13	14	PAS	AB131	PAS	13	PAS	14	PAS	AB131	PAS	13	PAS	14
M. smegmatis MC^2 155(WT)	1.250	>64	>64	>64	0.313	16	0.313	8	0.313	8	0.257 (SYN)		0.254 (SYN)		0.25 (SYN)	
M. tuberculosis H37Rv	0.125	>64	>64	>64	0.061	25	/		/		0.488 (SYN)		/		/	
M. bovis BCG-Pasteur	0.125	>64	>64	>64	/		/		0.020	3.1	/		/		0.161 (SYN)	
M. marinum BAA-535	0.250	>64	64	64	/		/		/		/		/		/	

[a]Abbreviations: PAS, para-aminosalicylic acid; SYN, synergism; "/" indicates no synergistic effect; FICI, fractional inhibitory concentration index (FICI ≤ 0.5 indicates a synergistic effect, 0.5 < FICI ≤ 4 indicates no interaction, and FICI > 4 indicates an antagonistic effect).

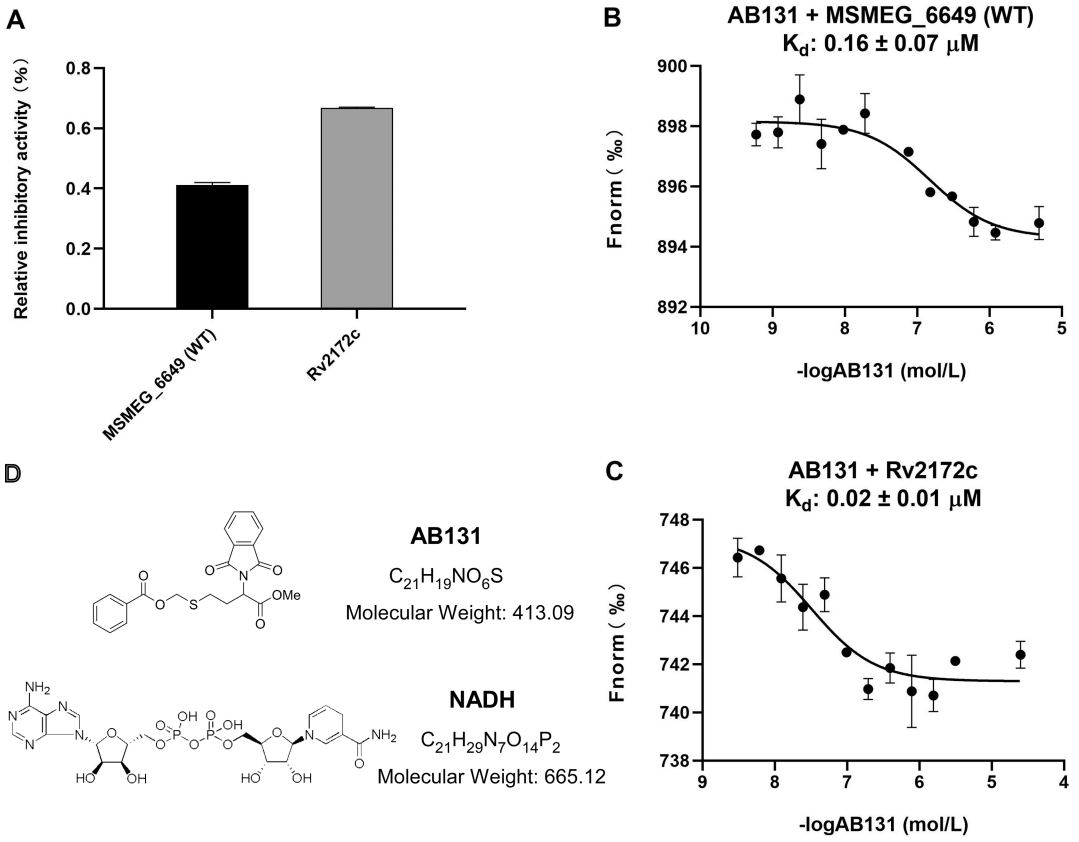

Figure 1. AB131 is a strong inhibitor of MSMEG_6649 and Rv2172c. (A) *In vitro* inhibitory effects of AB131 on the enzyme activities of wild-type MSMEG_6649 or Rv2172c and the enzyme activity of wild-type MSMEG_6649 or Rv2172c without adding compound AB131 used as a control. (B,C) Binding affinities of AB131 to wild-type MSMEG_6649 or wild-type Rv2172c evaluated by MST analyses. The concentration of wild-type MSMEG_6649 and Rv2172c is constant at 5 nM, while the tested compound concentration ranged from 24 nM to 800 μM (mean value ± SEM of three biological replicates, *P < 0.05; **P < 0.01). (D) Chemical structures of compound AB131 and NADH.

the candidate compound AB131 and PAS led to a significantly lower minimum inhibitory concentration (MIC) value (0.313 μg/mL) compared to the use of PAS (1.250 μg/mL) or AB131 (>64 μg/mL) alone, suggesting that AB131 acts as a sensitizer of PAS (Table 1 and Table S2). In comparison, AB131 can also moderately sensitize the other two antifolates SMX and TMP (Table S3).

To determine whether AB131 functions as a sensitizer by targeting MSMEG_6649 or Rv2172c, we performed *in vitro* measurements of the inhibitory activity of compound AB131 against both enzymes. Results showed that AB131 inhibited the enzyme activities of MSMEG_6649 and Rv2172c by 43 and 67%, respectively (Figure 1). We also performed checkerboard interaction assays on *M. smegmatis* MC^2 155, *M. tuberculosis* H37Rv, *M. bovis* BCG-Pasteur, and *Mycobacterium marinum* to evaluate the synergistic effects of AB131 and PAS. The results showed that the combination of AB131 and PAS had a synergistic interaction for all strains tested, as evidenced by the FICI values below 0.5 (Table 1). These findings were consistent with our enzyme activity results and

https://doi.org/10.1021/acsomega.3c05021
ACS Omega 2023, 8, 38406−38417

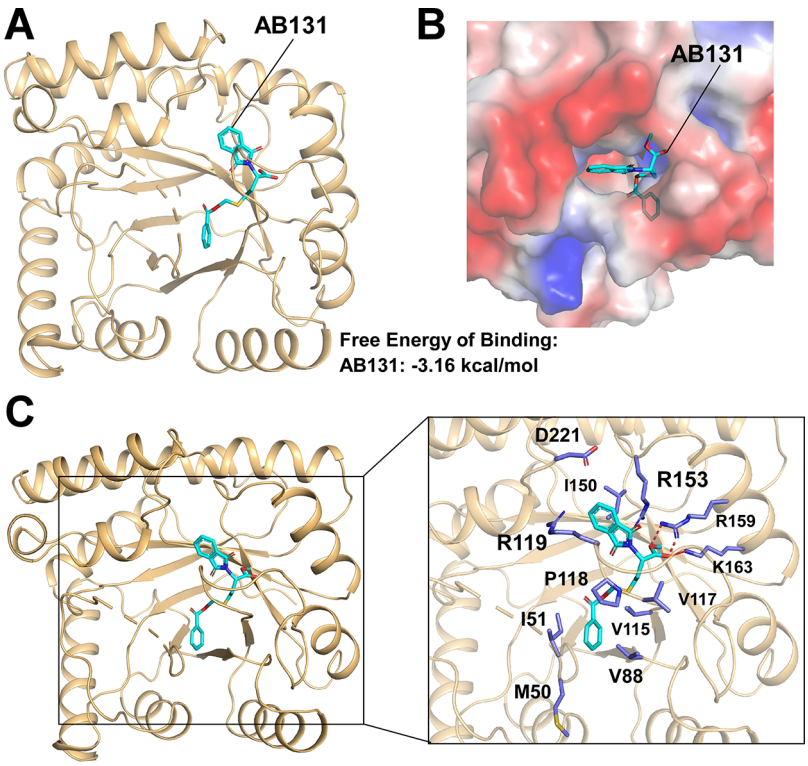

Figure 2. Molecular docking of MSMEG_6649 with AB131. (A) Structure model of MSMEG_6649 in complex with AB131 subjected to energy-favorable optimization. Cyan, AB131 carbon atoms; red, oxygen atoms; blue, nitrogen atoms. (B) Surface electrostatic potential of MSMEG_6649 in complex with AB131. (c) Zoomed-in view of key interactions between MSMEG_6649 and compound AB131.

further confirmed the potent sensitizing effect of AB131 on PAS. Meanwhile, since MTHFRs exist both in bacteria and humans, we also tested whether AB131 was specific to MTHFR MSMEG_6649 from bacteria, not human MTHFR that their 3D structure resembled (Figure S2).[22] The experimental results clearly showed that AB131 cannot target human MTHFR. Collectively, our antibacterial and enzyme activity assays strongly supported the notion that AB131 is an inhibitor of MSMEG_6649 and enhances the susceptibility of *M. smegmatis* to the antifolate PAS.

We next employed microscale thermophoresis (MST) analysis to investigate the direct interaction between AB131 and MSMEG_6649 or Rv2172c. The binding of AB131 to MSMEG_6649 was characterized by a sigmoidal curve with an estimated dissociation constant K_d of 0.16 μM, indicating a relatively strong binding affinity. Similarly, AB131 also exhibited a direct interaction with Rv2172c with a higher binding affinity with a K_d value of 0.02 μM (Figure 1). The results suggest that AB131 is a potent inhibitor of both MSMEG_6649 and Rv2172c, indicating its potential to impede the growth of mycobacteria and possibly serve as a sensitizer of antitubercular drugs.

Molecular Docking of AB131 with MSMEG_6649. To set the foundation for the optimization of AB131 for improved druggability, we attempted to uncover the interactions between compound AB131 and MSMEG_6649 by determining the cocrystal structure of MSMEG_6649 with AB131. Despite employing both cocrystallization and soaking methods, our endeavors to obtain the cocrystals of MSMEG_6649 with compound AB131 were unsuccessful, possibly accounting for improper crystal packing and the poor aqueous solubility of AB131. Instead, we employed a computer-aided molecular docking method to predict the interactions based on the cocrystal structure of MSMEG_6649 with NADH. The MSMEG_6649 enzyme adopted an architecture of a $(\beta\alpha)_8$ barrel in the structure. Our molecular docking studies showed that AB131 can fit the NADH binding pocket well with an estimated free binding energy of −3.16 kcal/mol (Figure 2), while a series of surrounding hydrophilic and hydrophobic amino acid residues (M50, I51, V88, V115, V117, P118, R119, I150, R153, R159, K163, and D221) may be indispensable for the binding of the AB131 molecule. In addition, we found that residues R119, I150, R153, R159, K163, and D221 played key roles in NADH binding and formed a hydrophilic cleft, indicating that the predicted interaction residues were correct. Specifically, residues R153, R159, and K163 may form hydrogen bonding interactions with the oxygen atoms of AB131, thus stabilizing the binding between them. Our results collectively suggest that AB131 inhibited the enzyme activity of MSMEG_6649 most likely through occupying the NADH binding pocket of MSMEG_6649.

Validation of Critical Residues for AB131 Binding by Mutagenesis. Following the results of the aforementioned molecular docking study, we conducted MST binding analysis and enzymatic activity assays to confirm the necessity of the predicted AB131 binding pocket residues. Our findings indicated that the V115A and K163A mutants of MSMEG_6649 displayed no observable binding affinity to AB131 (K_d > 50 mM), while the binding affinities of the V117A and P118A mutants significantly reduced (K_d= 3.53 ± 1.16 μM for V117A and 6.15 ± 1.49 μM for P118A) in comparison to the wild-type MSMEG_6649 (K_d = 0.16 ± 0.07 μM), which was approximately 20-fold lower (Figure 2). Surprisingly, the R119A mutation showed a similar binding

https://doi.org/10.1021/acsomega.3c05021
ACS Omega 2023, 8, 38406−38417

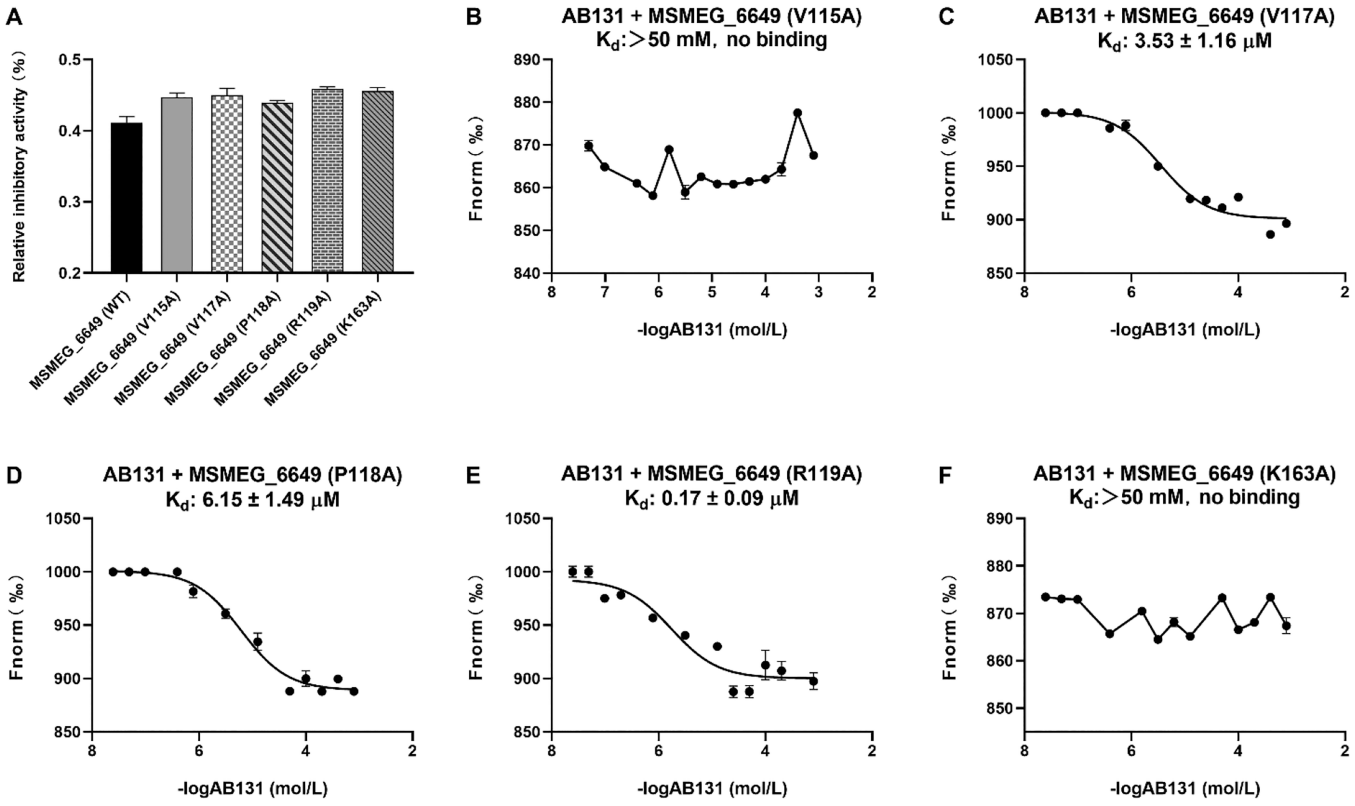

Figure 3. *In vitro* inhibitory effects of compound AB131 against the enzyme activities and binding affinities of MSMEG_6649 mutants (mean value ± SEM of three biological replicates, $*P < 0.05$; $**P < 0.01$). (A) *In vitro* inhibitory effects of AB131 on wild-type MSMEG_6649 and its mutants (V115A, V117A, P118A, R119A, and K163A) and the enzyme activity of wild-type MSMEG_6649 without adding compound AB131 used as a control. (B–F) Binding affinities of AB131 to MSMEG_6649 mutants assessed by MST analyses. The concentrations of MSMEG_6649 mutants are constant at 5 nM, while the tested compound concentration ranged from 24 nM to 800 μM (mean value ± SEM of three biological replicates, $*P < 0.05$; $**P < 0.01$).

affinity (K_d = 0.17 ± 0.09 μM) to that of wild-type MSMEG_6649 against AB131, suggesting that residue R119 may not play a crucial role in the binding of AB131.

In accordance with the MST results, compound AB131 displayed significantly reduced inhibitory activities to MSMEG_6649 mutants V115A, V117A, P118A, and K163A of MSMEG_6649 compared to the wild-type enzyme (Figure 3). However, the R119A mutant did not appear to have an obvious effect on enzyme activity, possibly because R119 did not directly participate in the binding of AB131. Overall, the residues V115, V117, P118, and K163, which were predicted to be associated with AB131 binding by molecular docking, were confirmed to be vital in stabilizing the MSMEG_6649-AB131 complex. The complex was formed primarily by hydrophobic and hydrophilic interactions between AB131 and MSMEG_6649, as supported by both MST and enzyme activity assays.

Evaluation of the Sensitizing Effects of AB131 and Its Derivatives. To further optimize the pharmaceutical features of compound AB131, we *de novo* synthesized the lead compound AB131 and a series of its derivatives based on the identified key residues of the AB131 binding pocket in MSMEG_6649 (Figure S3).[10] Both enzyme activity inhibitory assays and antibacterial assays were performed to screen the priority candidates. Compounds **1**, **12**, **13**, **17**, and **19** exhibited moderate inhibitory effects toward the enzyme activities of MSMEG_6649, while coadministration of compound **13** or **14** with PAS showed relative high susceptibility to PAS against wild-type *M. smegmatis* MC^2 155 in comparison with the rest (Figure 4, Table 1, and Table S4). Taken together with these data, compounds **13**, **14**, and AB131 were selected for further antibacterial activity evaluations (including *M. tuberculosis* H37Rv, *Mycobacterium bovis* BCG-Pasteur, and *M. marinum*). The results showed that coadministration of AB131 and PAS displayed higher antibacterial activities against *M. tuberculosis* H37Rv than compound **13** or **14** and PAS (Table 1). Collectively, these *in vitro* antibacterial activity results strongly suggested that compound AB131 can act as a sensitizer of antifolate PAS to inhibit mycobacteria.

To optimize the pharmacological properties of AB131, we synthesized AB131 and a series of derivatives (**1**–**22**) rationally designed based on the key residues identified in the AB131 binding pocket of MSMEG_6649 (Figure S3), which were subjected to the enzyme inhibitory assay and synergistic antimycobacterial assay with PAS. Compounds **1**, **12**, **13**, **17**, and **19** exhibited moderate inhibitory effects on the enzyme activities of MSMEG_6649. When compound **13** or **14** was coadministered with PAS, *M. smegmatis* MC^2 155 displayed relatively higher susceptibility to PAS compared to the other derivatives (Figure 4, Table 1, andTable S3). Therefore, the AB131 derivatives **13** and **14** together with AB131 were selected for antimycobacterial evaluation against *M. tuberculosis* H37Rv, *Mycobacterium bovis* BCG-Pasteur, and *M. marinum*. The results revealed that all three compounds had comparable effects in enhancing the activity of PAS against *M.*

https://doi.org/10.1021/acsomega.3c05021
ACS Omega 2023, 8, 38406–38417

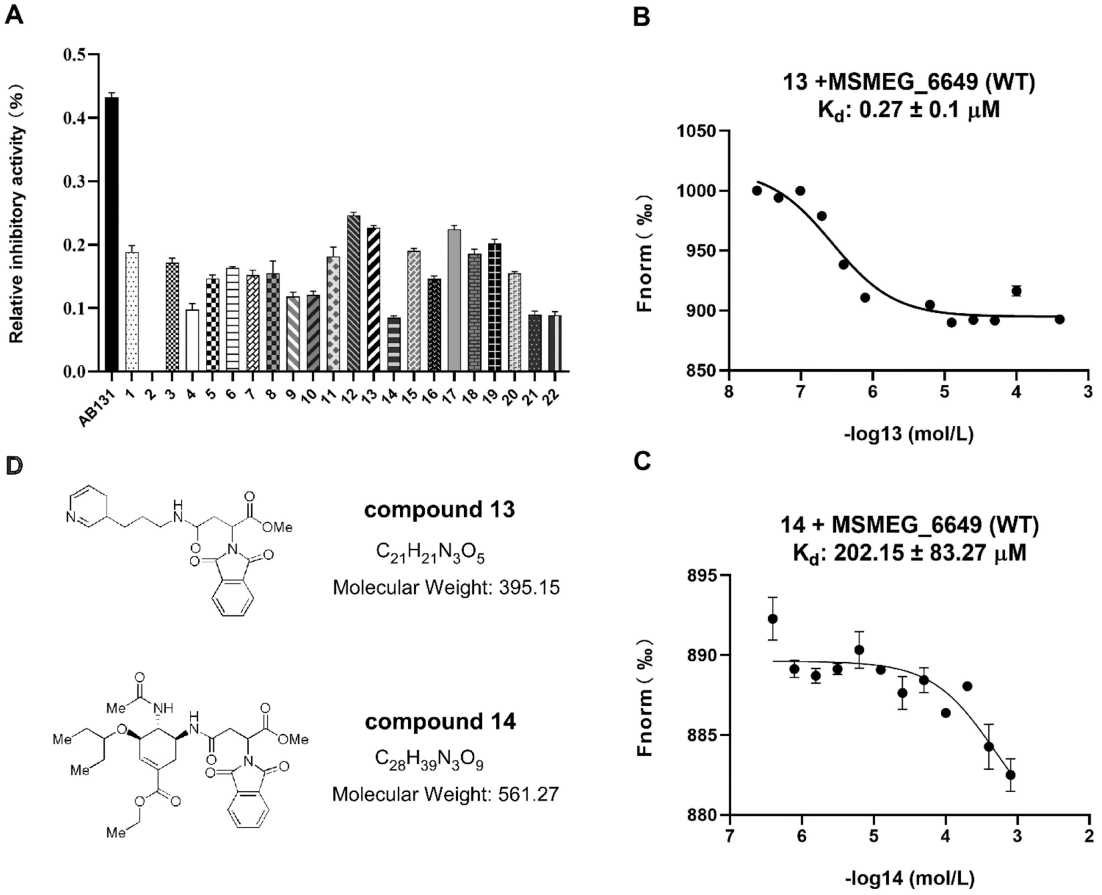

Figure 4. *In vitro* inhibitory effects of compound AB131 and its derivatives against the enzyme activities and binding affinities of wild-type MSMEG_6649. (A) *In vitro* inhibitory activities of AB131 and its derivatives to wild-type MSMEG_6649 and the enzyme activity of wild-type MSMEG_6649 without adding AB131 and its derivatives used as a control. (B,C) Binding affinities of AB131 derivative compound 13 or 14 to wild-type MSMEG_6649 measured by MST assays. The concentration of wild-type MSMEG_6649 is constant at 5 nM, while the tested concentration of compound 13 or 14 ranged from 24 nM to 800 μM (mean value ± SEM of three biological replicates, $^{*}P < 0.05$; $^{**}P < 0.01$). (D) Chemical structures of AB131 derivative compounds 13 and 14.

Table 2. Antimycobacterial Activities of AB131 Combined with TB Drug PAS against Wild-Type *M. smegmatis* MC^2 155, *M. smegmatis* MC^2 155 Δ*MSMEG_6649,* and Its Complementary Strains[a]

	MIC (μg/mL)				
	drug alone		drug in combination		
mycobacterial strains	PAS	AB131	PAS	AB131	interpretation
wild-type *M. smegmatis* MC^2 155	1.25	>64	0.313	16	SYN
MC^2 155 Δ*MSMEG_6649::WT6649*	1.25	>64	0.625	32	
MC^2 155 Δ*MSMEG_6649::WT6649*	1.25	>64	0.313	16	SYN
MC^2 155 Δ*MSMEG_6649::WT6649(V115A)*	1.25	>64	0.313	32	
MC^2 155 Δ*MSMEG_6649::WT6649(V117A)*	1.25	>64	0.313	24	SYN
MC^2 155 Δ*MSMEG_6649::WT6649(P118A)*	1.25	>64	0.313	24	SYN
MC^2 155 Δ*MSMEG_6649::WT6649(R119A)*	1.25	>64	0.313	16	SYN
MC^2 155 Δ*MSMEG_6649::WT6649(K163A)*	1.25	>64	0.313	32	

[a]Abbreviations: PAS, para-aminosalicylic acid; SYN, synergism; FICI, fractional inhibitory concentration index (FICI ≤ 0.5 indicates a synergistic effect, 0.5 > FICI ≤ 4 indicates no interaction, and FICI > 4 indicates an antagonistic effect).

smegmatis MC^2 155. Among the tested compounds, the coadministration of AB131 and PAS displayed the highest antibacterial activity against *M. tuberculosis* H37Rv, while compounds **13** and **14** did not exhibit any sensitizing effect on *M. tuberculosis* H37Rv (Table 1). Conversely, compound **14** strongly sensitized the activity of PAS against *Mycobacterium bovis* BCG-Pasteur, with an FICI value of 0.161, whereas compounds **13** and AB131 did not show such activity as in Table 1.

To demonstrate the whole-cell antibacterial activity driven by inhibiting the proposed target MSMEG_6649 *in vivo*, we constructed the *M. smegmatis* MC^2 155 ΔMSMEG_6649 strain (Figure S4) and its complementary strains to investigate the effects of increasing susceptibility to PAS caused by AB131. Our results showed that the coadministration of PAS and

https://doi.org/10.1021/acsomega.3c05021
ACS Omega 2023, 8, 38406−38417

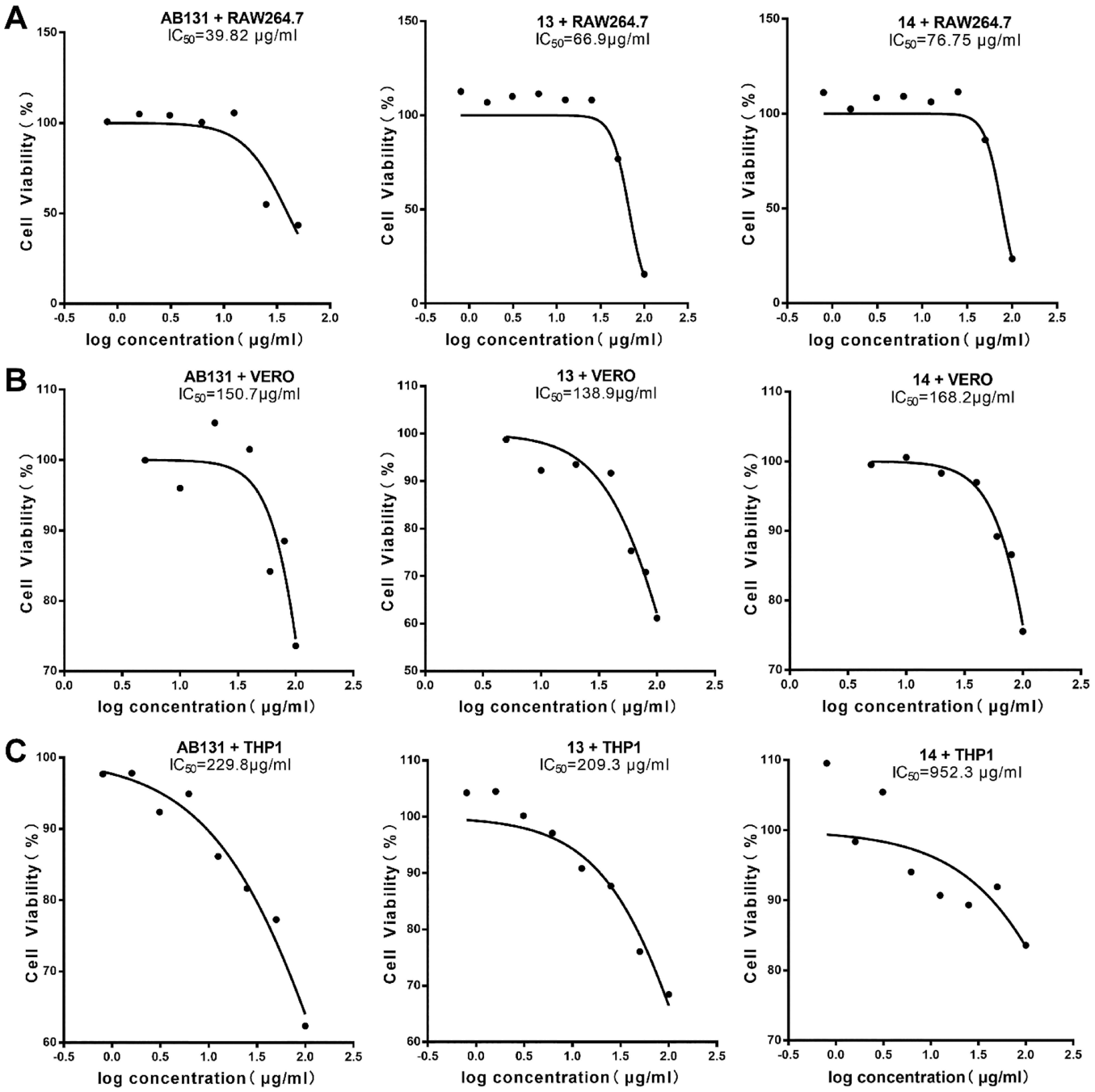

Figure 5. Cytotoxicity evaluation of AB131 and its derivatives compound 13 or 14 to the Raw264.7, Vero, and THP-1 cells. (A−C) Cell viabilities of Vero cells, RAW264.7 cells, and THP-1 cells subjected to the compound AB131 or compound 13 or 14 at concentrations ranging from 0.8 to 100 μg/mL.

AB131 did not exhibit a significant sensitizing effect on *M. smegmatis* MC^2 155 ΔMSMEG_6649 when compared to the wild-type *M. smegmatis* MC^2 155. Additionally, there was no sensitizing activity observed for the *M. smegmatis* complementary strains harboring V115A, R119A, or K163A MSMEG_6649 mutations. For the complementary V117A and P118A strains, the combinatory administration of PAS with AB131 displayed a weak sensitizing effect (Table 2). These results verified that compound AB131 can sensitize the antibacterial activity of PAS against mycobacteria by directly inhibiting the proposed target MSMEG_6649 *in vivo*.

The Cytotoxicity Evaluation of AB131 and Its Derivatives. As AB131 and its derivatives **13** and **14** can enhance the inhibitory activity of PAS against mycobacteria, we next assessed their cytotoxicity against three human immune cell lines, namely, Vero, Raw264.7, and mycobacteria-infected THP-1 macrophage cell lines by a CCK-8 assay. The results shown in Figure 5 indicate that AB131, compound **13**, and compound **14** did not display significant cytotoxicity toward human cells, with IC_{50} values above 35 μg/mL. These values are notably higher than the MICs of AB131, compound **13**, and compound **14** when combined with PAS, suggesting

https://doi.org/10.1021/acsomega.3c05021
ACS Omega 2023, 8, 38406−38417

that they have promising potential as antimycobacterial drug sensitizers.

CONCLUSIONS

The sequence and three-dimensional structure of mycobacterial MTHFR are highly conserved in most mycobacteria but differ from other bacteria, making mycobacterial MTHFR an important drug target for developing new anti-infective drugs.[10] Targeting mycobacterial MTHFR could be a novel approach to controlling antibiotic-resistant strains. In this study, we conducted high-throughput virtual screening based on the cocrystal structure of MSMEG_6649 with NADH and identified a promising lead compound, AB131. Its structural derivatives were synthesized and optimized, exhibiting high inhibitory activities against MSMEG_6649 and showing good synergistic effects when combined with PAS. Further structure optimizations and animal studies will be necessary to evaluate and enhance its pharmaceutical features. This discovery offers new insights for effectively addressing latent infections in drug-resistant tuberculosis.

MATERIALS AND METHODS

Chemicals, Plasmids, Bacteria Culture, and Cell Lines. 5,10-Methylene-5,6,7,8-tetrahydrofolic acid (5,10-CH_2-THF) and 5-methyl-5,6,7,8-tetrahydrofolic acid (5-CH_3-THF) were purchased from Schircks Laboratories (Jona, Switzerland). The concentrations of 5,10-CH_2-THF, NADH, and NADPH (Sigma-Aldrich) were determined spectrophotometrically at 294 and 340 nm. *E. coli* and mycobacterial strains were grown in an LB or Middlebrook 7H9 medium with the appropriate antibiotics. The Vero (ATCC CCL-81), Raw264.7 (ATCC TIB-71), and THP-1 (ATCC TIB-202) cell lines used for CCK-8 cytotoxicity assays were purchased from American Type Culture Collection (ATCC).

Synthesis of Compound AB131 and Its Derivatives. The target product was synthesized according to the following procedures.

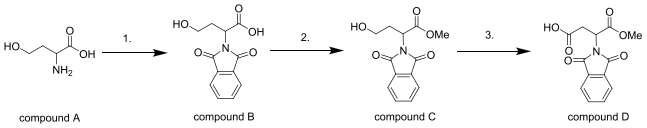

Step 1: Na_2CO_3 (899 mg, 8.48 mmol, 1.0 equiv) followed by *N*-carbethoxyphthalimide (1.86 g, 8.48 mmol, 1.0 equiv) was added to a flask containing the solution of compound A (1.01 g, 8.48 mmol, 1.0 equiv) in H_2O (6.3 mL) at room temperature. The reaction mixture was stirred at room temperature for a further 3h. Then, the reaction mixture was acidified with cold 1 N HCl to a pH of 2 and extracted with EtOAc (3 × 50 mL). The organic extracts were combined, washed with brine, dried over Na_2SO_4, filtered, and concentrated in vacuum to afford the crude product compound B. The crude product compound B could be used for the next step without further purification.

Step 2: Dicyclohexylamine (0.85 mL) was added to a flask containing the solution of compound B (0.5 g, 8.48 mmol, 1.0 equiv) in EtOH (6.3 mL) at room temperature. The reaction was stirred at room temperature until the reaction was fully completed. Then, the solvent was evaporated in vacuo to afford the dicyclohexylamine salt product in a white solid form. CH_3I (0.79 mL) was added to a solution of the combined white solid in DMF (20 mL) at room temperature. The reaction mixture was stirred at room temperature overnight; then, water (100 mL) was added followed by EtOAc. The layers were separated, and the aqueous portion was extracted with EtOAc (3 × 20 mL). The organic extracts were combined, washed with brine, dried over Na_2SO_4, filtered, and concentrated in vacuo. Purification by flash chromatography (PE/EA 3:1) afforded compound C in an oil form.

Step 3: Compound C (100 mg, 0.379 mmol, 1.0 equiv) was added to a flask containing the solution of MeCN (3.8 mL) and phosphate buffer (2.4 mL) at room temperature. Then, the reaction was heated to 35 °C. TEMPO (8.3 mg, 0.053 mmol, 0.14 equiv) supplemented with $NaClO_2$ (137 mg in 0.52 mL of water) and dilute bleach (1.06 mL 7.5% in 28.6 mL of water) were added to the reaction mixture. The reaction was stirred at room temperature until the reaction was fully completed. Then, the reaction was quenched with cold $Na_2S_2O_3$ (1.525 g in 25 mL of water) and stirred for 5 min. Then, the reaction mixture was acidified with cold 2 N HCl to a pH of 3−4 and extracted with EtOAc (3 × 50 mL). The organic extracts were combined, washed with brine, dried over Na_2SO_4, filtered, concentrated *in vacuo*, and purified by flash chromatography to afford compound D with 63.6% yield.

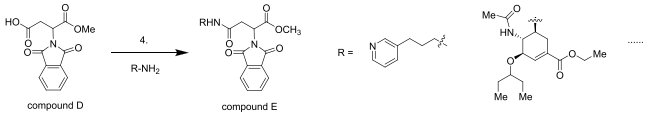

Step 4: Compound D (20 mg, 0.072 mmol, 1.0 equiv), compound R_1-NH_2, and *N*-methylimidazole (21 μL, 0.252 mmol, 3.5 equiv) were combined and dissolved in 10 mL of MeCN with an addition of 31 mg of TCFH (0.086 mmol, 1.2 equiv) in a single portion. The reaction was stirred until it was complete by HPLC. The reaction was then diluted with 6 mL of EtOAc and 4 mL of water. The layers were separated, the aqueous layer was extracted with 4 mL of EtOAc, and the combined organics were washed with 4 mL of water, dried with $MgSO_4$, filtered, and concentrated before purification by silica gel chromatography to give the final product with 71.1% yield.

Gene Cloning, Site-Directed Mutagenesis, Expression, and Purification of *MSMEG_6649*. The 5,10-methylenetetrahydrofolate reductase genes *MSMEG_6649* from *M. smegmatis* and *Rv2172c* from *M. tuberculosis* H37Rv were first amplified from the genomic DNA of *M. smegmatis* MC^2 155 or *M. tuberculosis* H37Rv and cloned into the protein expression vector pET28a using *Nhe*I and *Hind*III to yield pET28a-*MSMEG_6649* or pET28a-*Rv2172c*, which was transformed into *E. coli* BL21(DE3) (Invitrogen) after DNA sequencing, respectively. The correct transformant was inoculated and incubated at 37 °C in an LB medium to an OD_{600} of 1.0−1.2. Isopropyl-β-d-thiogalactoside (IPTG) was subsequently added to the final concentration of 0.5 mM to induce protein expression, and then, the culture was incubated for 16−20 h at 16 °C. Bacterial cells were harvested by centrifugation (5,000*g*; 15 min at 4 °C), resuspended in buffer A (10 mM Tris-HCl, pH 8.0, 200 mM NaCl, and 5% glycerol), and disrupted using an EmulsiFlex-C5 cell disruptor (Avestin). Recombinant MSMEG_6649 or Rv2172c proteins were first purified over a 5 mL column of Ni^{2+}-NTA-agarose (Qiagen) and further purified by a HiLoad 16/60 Superdex 200 prep-grade column (GE Healthcare) in 10 mM Tris-HCl, pH 8.0, 50 mM NaCl, 5 mM $MgCl_2$, and 1 mM dithiothreitol (DTT). The fractions were then evaluated by SDS-PAGE. The pure fractions were collected and concentrated using centrifugal

https://doi.org/10.1021/acsomega.3c05021
ACS Omega 2023, 8, 38406−38417

ultrafilters (EMD Millipore) and stored at −80 °C. For site-directed mutations, a one-step PCR method and a QuikChange site-directed mutagenesis kit (Agilent) were used, and the mutated proteins were expressed and purified in the same way as the wild-type proteins.

Construction of the *M. smegmatis* Mutant and Complementary Strains. The gene *MSMEG_6649* in *M. smegmatis* MC^2 155 was replaced with a hygromycin-resistant fragment through the allelic exchange method described previously with minor modifications.[28] In brief, one fragment with the upstream and downstream regions of *MSMEG_6649* was amplified from the genomic DNA of *M. smegmatis* MC^2 155 with the primers for constructing the knockout strain. The PCR product was then cloned into the vector pYUB854 after restriction enzyme digestion, generating the knockout plasmid pYUB854-*MSMEG_6649*. Subsequently, competent cells of *M. smegmatis* MC^2 155 were prepared and transformed. The positive hygromycin-resistant colonies were screened and verified by DNA sequencing with the primers for verification of the *MSMEG_6649* knockout strain. For constructing the complementary strain, the wild-type *MSMEG_6649* with its native promoter was amplified and cloned into the integrative vector pMV306, resulting in the complementary plasmid pMV306-*MSMEG_6649(WT)*. After being sequenced correctly, the plasmid was transformed into the *M. smegmatis* MC^2 155 Δ*MSMEG_6649* strain. The positive complementary strains were screened by hygromycin- and kanamycin-resistant screening. The *MSMEG_6649* site-directed mutants were generated using a QuikChange site-directed mutagenesis kit (Agilent) on the basis of pMV306-*MSMEG_6649(WT)* and complemented into the *M. smegmatis* MC^2 155 Δ*MSMEG_6649* strain as the wild-type one. The primers used for constructing the knockout and complementary strains are listed in Table S1.

***In Vitro* Enzyme Activity Assays.** The enzyme activity assays for MSMEG_6649 and its derivatives were assessed following a previous method described for *Eco*MTHFR.[7,21] Briefly, the activities of MSMEG_6649 and its mutants were measured by monitoring the change in NADH/NADPH absorbance at 340 nm for 5 s at 25 °C in PBS buffer purged with N_2 gas. The concentration of 5,10-CH_2-THF was 500 μM while keeping NADH at 100 μM and AB131 or its derivatives at 100 μM. Conversions of 5,10-CH_2-THF and NADH to 5-CH_3-THF and NAD^+ were determined at 340 nm using a millimolar extinction coefficient of 6.22 M^{-1} cm^{-1}.

The enzyme activity assays for the catalytic domain of human MTHFR encompassing amino acids Met1-Arg325 (referred to as human MTHFR (1−325)) were performed in strict accordance with the physiological forward assay reported previously.[22,29,30] Briefly, the purified human MTHFR (1−325) (commercially available in Yubo, Shanghai, China) was dissolved in buffer A (10 mM Tris-HCl, pH 8.0, 200 mM NaCl, and 5% glycerol), and the specific enzyme activity was measured under substrate concentrations (500 μM 5,10-CH_2-THF, 100 μM NADPH, and 100 μM FAD, Sigma-Aldrich), with and without the addition of the candidate compounds (100 μM). The data were analyzed using GraphPad Prism, and the mean values with standard deviations were plotted. The kinetic constants K_m and V_{max} were calculated using eq 1.

$$V_0 = V_{max}[S]/(K_m + [S]) \quad (1)$$

where V_0 is the initial velocity, $[E]$ is the enzyme concentration, $[S]$ is the substrate concentration, V_{max} is the maximum velocity, and K_m is the Michaelis constant.

Molecular Docking-Based Virtual Screening and Molecular Docking. The compound library was obtained from Specs, which was comprised by 202,294 compounds (https://www.specs.net). Two molecular docking programs, the Glide module in Schrodinger Maestro 2019 and AutoDock Vina were combined for improving the accuracy of docking prediction. Initially, the compounds were prepared using the module of Ligand Prepare in Schrodinger Maestro 2019. Hydrogens were added, and 3D geometries, ionization, and tautomeric states were generated. Then, the ligands were minimized using the OPLS 2005 force field and docked into the NADH binding pocket within the cocrystal structure of the MSMEG_6649−NADH complex (PDB ID 7WMW). Meanwhile, the MSMEG_6649 was prepared by using the module of Protein Preparation Wizard in Schrodinger Maestro 2019. The waters were eliminated from the protein, and the polar hydrogens were added. Meanwhile, the protonation states of all residues had been considered involving His protonated to HID, and the Asp, Arg, Glu, and Lys residues were preprocessed to deprotonated states. Receptor grids were generated using Receptor Grid Generation, and the binding site was generated within a radius of 20 Å at the center from the ligand, including several key amino acid residues.

The first round of virtual screening was conducted by the Glide program in the standard precision (SP) and extra precision (XP) mode. Other parameters were as default. As a result, the docking score was considered as the initial evaluation criteria. In addition, the optimal docking orientation and interaction of compounds in the binding site of protein were visually inspected to analyze the protein−ligand interaction. After the first docking-based virtual screening, the compounds were further filtered by AutoDock. Finally, according to binding energy and predicted interactive mechanisms between the ligands and protein, the ligands with the best binding conformation were selected for further biological evaluation.

For the molecular docking studies of compound AB131 in this study,[31] generally, the crystal structure of *apo* MSMEG_6649 (PDB ID 7WMW) was docked with compound AB131. The molecule was added with nonpolar hydrogens and assigned partial atomic charges using AutoDockTools (ADT).[31] The coordinates of AB131 in the MSMEG_6649 structure were generated based on the coordinates of NADH in the cocrystal structure of MSMEG_6649 in complex with NADH (PDB ID 7WMZ) using the CORINA Classic online service. A grid box with 40 × 40 × 40 grid points and a 0.2 Å grid spacing centered roughly at the NADH binding position was used as the searching space. One hundred runs of the Larmarckian genetic algorithm were performed to search the protein−ligand interactions. The results were clustered and ranked. Result analyses and figure rendering were performed by using PyMOL.

Antibacterial Activity Assay. The antibacterial activity assay was carried out through measuring the minimal inhibitory concentrations (MICs) based on broth microdilution assays. In general, 100 μL of Middlebrook 7H9 broth (BD Biosciences) was loaded per well containing a starting cell density of 1−5 × 10^5 CFU/mL *M. smegmatis* MC^2 155 (*Msm*), *M. tuberculosis* H37Rv (*Mtb*), *Mycobacterium bovis* BCG-pasteu

https://doi.org/10.1021/acsomega.3c05021
ACS Omega 2023, 8, 38406−38417

(*Mbo*), and *Mycobacterim marinum* (*Mma*) and 20 μL 0.1 mg/mL resazurin sodium salt into 96-well plates (YB-96U, Yueyi Biotech), and then, 100 μL of 7H9 broth containing 2-fold serial dilutions of the tested compounds (PAS (the final concentrations are at 0, 0.039, 0.078, 0.157, 0.313, 0.625, 1.25, 2.5, and 5.0 μg/mL), AB131 and 34 other energy-favorable candidate compounds, and AB131 derivatives including compounds **13** and **14** (the final concentrations are at 0, 1, 2, 4, 8, 16, 32, 64, and 128 μg/mL, respectively)) was added at 37 °C. PAS, rifampin (Rif), and isoniazid (INH) were used to be the positive controls. After an incubation time of 2 days, the MIC values were quantified, and the results were the mean values from three biological replicates.

Checkerboard interaction assays based on broth microdilution assays were designed in a checkerboard format and used to evaluate antibacterial activities of combinations of PAS and compound AB131, compound **13**, or **14**. In general, the experiments were performed in three biological replicates and analyzed in all pairwise combinations of PAS at 0, 0.039, 0.078, 0.157, 0.313, 0.625, 1.25, 2.5, and 5.0 μg/mL with the tested compound (AB131, compound **13**, or **14**) at 0, 1, 2 4, 8, 16, 32, 64, and 128 μg/mL. FICI is the fractional inhibitory concentration index (FICI ≤ 0.5 indicates a synergistic effect (synergism was abbreviated to SYN), 0.5 h FICI ≤ 4 indicates no interaction, and FICI > 4 indicates an antagonistic effect).[32,33]

Microscale Thermophoresis (MST) Binding Assay. To measure the binding affinities between wild-type Rv2172c, wild-type MSMEG_6649, and its site-directed mutants with NADH or compound AB131 or compound **13** or **14**, the MST binding assays were carried out as described previously.[34] Briefly, the NT- 647-NHS dye from the Monolith NTTM Protein Labeling Kit RED-NHS was first used to label the wild-type Rv2172c, wild-type MSMEG_6649, and their mutants by following the manufacturer's instructions (NanoTemper Technologies). The labeled Rv2172c, MSMEG_6649, or their mutants were mixed with 1:2 serial dilutions of NADH or AB131 or compound **13** or **14** in PBS buffer (pH 7.8) with 0.05% Tween-20 and incubated for 15 min at 25 °C and then loaded into NT.115 premium-coated capillaries from NanoTemper Technologies. MST assays were carried out by exactly following the manufacturer's protocol, and data analyses were performed by MO Affinity Analysis software version 2.3 and GraphPad Prism 7 software.

Cytotoxicity Assay. A CCK-8 cell activity test kit (CK04, Peer Chemistry) was used to perform the cytotoxicity assays, and the experimental procedures were followed as the protocol provided by the manufacturer with minor modifications. In brief, Vero and Raw264.7 cells were first inoculated into the 96-well plates with 2×10^5 or 4×10^5 cells per well, respectively, and incubated for 24 h at 37 °C, mixed with PAS (the final concentrations ranged at 0.03−7.5 μg/mL) and compound AB131, compound **13**, or **14** (the final concentrations ranged at 0.8−100.0 μg/mL) for 24 h in a 37 °C, 5% CO_2 incubator. Afterward, 10 μL/well of the CCK-8 solution was added to each well. Samples were protected from light and incubated for 2 h at 37 °C. The cell vitality was determined by the absorbance at 450 nm using a SpectraMax i3X (Biotek Synergy LX) and analyzed by GraphPad Prism 7 software. For testing the cytotoxicity to THP-1 cells, 100 nM phorbol myristate acetate (PMA) was essential to be added into the 96-well plate in order to induce the THP-1 cells to macrophage; other procedures were similar to Vero and Raw264.7 cells. The experiments were performed in triplicate.

Statistical Analysis. Data in this study were shown as mean values ± SEM of three biological replicates. One-way ANOVAs with Tukey's comparisons were carried out for statistical analysis using the GraphPad Prism 7.0 program.

■ ASSOCIATED CONTENT

Supporting Information

The Supporting Information is available free of charge at https://pubs.acs.org/doi/10.1021/acsomega.3c05021.

Chemical structures of 35 energy-favorable candidate compounds (Figure S1); *in vitro* inhibitory effects of AB131 or its derivatives compound 13 or 14 on the enzyme activities of wild-type MSMEG_6649 or human MTHFR (1−325) (Figure S2); chemical structures of NADH, AB131, and its derivatives (compounds 1−22) (Figure S3); identification of *M. smegmatis* MC^2 155 Δ*MSMEG_6649* (Figure S4); primer sequences used in this study (Table S1); activities of 35 energy-favorable candidate compounds combined with current TB drug PAS against wild-type *M. smegmatis* MC^2 155 (Table S2); antimycobacterial profile of AB131 and its derivatives combined with current TB drug SMX or TMP against wild-type *M. smegmatis* MC^2 155 (Table S3); antimycobacterial profile of AB131 and its derivatives combined with current TB drug PAS against wild-type *M. smegmatis* MC^2 155 (Table S4) (PDF)

■ AUTHOR INFORMATION

Corresponding Authors

Zhuo Shang − *School of Pharmaceutical Sciences, Shandong University, 250100 Jinan, China*; Email: zshang@sdu.edu.cn

Wei Lin − *State Key Laboratory of Bioreactor Engineering, East China University of Science and Technology, 200237 Shanghai, China; School of Pharmacy and Department of Pathogen Biology, School of Medicine & Holistic Integrative Medicine, Nanjing University of Chinese Medicine, 210023 Nanjing, China; Jiangsu Collaborative Innovation Center of Chinese Medicinal Resources Industrialization, 210023 Nanjing, China*; orcid.org/0000-0002-2940-6966; Email: weilin@njucm.edu.cn

Authors

Jiacong Li − *Department of Pathogen Biology, School of Medicine & Holistic Integrative Medicine and School of Pharmacy, Nanjing University of Chinese Medicine, 210023 Nanjing, China; State Key Laboratory of Bioreactor Engineering, East China University of Science and Technology, 200237 Shanghai, China*

Yong Nian − *School of Pharmacy, Nanjing University of Chinese Medicine, 210023 Nanjing, China*

Jian Liu − *School of Pharmacy, Nanjing University of Chinese Medicine, 210023 Nanjing, China*; orcid.org/0000-0001-9482-9036

Mingxia Yang − *Department of Pathogen Biology, School of Medicine & Holistic Integrative Medicine, Nanjing University of Chinese Medicine, 210023 Nanjing, China; The Center for Microbes, Development and Health, Institut Pasteur of Shanghai, Chinese Academy of Sciences, 200031 Shanghai, China*

https://doi.org/10.1021/acsomega.3c05021
ACS Omega 2023, 8, 38406−38417

Yuanling Jin − *Department of Pathogen Biology, School of Medicine & Holistic Integrative Medicine, Nanjing University of Chinese Medicine, 210023 Nanjing, China*
Xiaoman Kang − *CAS Key Laboratory of Synthetic Biology, Centre of Excellence for Molecular Plant Sciences, Chinese Academy of Sciences, 200032 Shanghai, China*
Haodong Xu − *School of Pharmacy, Nanjing University of Chinese Medicine, 210023 Nanjing, China*

Complete contact information is available at: https://pubs.acs.org/10.1021/acsomega.3c05021

Author Contributions

○J.Li, Y.N., J.Liu, and M.Y. contributed equally to this work.

Author Contributions

W.L. performed conceptualization, methodologies, software, validation, supervision, and writing of the original draft. Y.N., J.Liu, M.Y., Y.J., X.K., H.X., and W.L. performed the investigation. Y.N., J.Liu, and W.L. performed investigation and data curation. Z.S. and W.L. reviewed and edited the manuscript.

Funding

This work was financially supported by the National Natural Science Foundation of China (32270192, 82072240, and 82204192), the Natural Science Foundation of Jiangsu Province (BK20220471 to Y.N.), the Open Funding Project of the State Key Laboratory of Bioreactor Engineering to W.L., the Open Projects of the State Key Laboratory of Drug Research, Shanghai Institute of Materia Medica, Chinese Academy of Sciences (no. SIMM2205KF-15 to W.L. and no. SIMM2205KF-10 to Y.N.), the Open Project of Chinese Materia Medica First-Class Discipline of Nanjing University of Chinese Medicine (no. 2020YLXK008 to W.L.), the Fok Ying Tung Education Foundation to W.L., and Nanjing University of Chinese Medicine (XPT82204192) to Y.N.

Notes

The authors declare no competing financial interest.

■ ACKNOWLEDGMENTS

We thank the staff at the experiment center for science and technology of Nanjing University of Chinese Medicine for experimental support.

■ REFERENCES

(1) Bagcchi, S. WHO's Global Tuberculosis Report 2022. *Lancet Microbe* **2023**, *4*, No. e20.
(2) Nguyen, L. Antibiotic resistance mechanisms in *M. tuberculosis*: an update. *Arch. Toxicol.* **2016**, *90*, 1585−1604.
(3) Lee, M. N.; Takawira, D.; Nikolova, A. P.; Ballou, D. P.; Furtado, V. C.; Phung, N. L.; Still, B. R.; Thorstad, M. K.; Tanner, J. J.; Trimmer, E. E. Functional role for the conformationally mobile phenylalanine 223 in the reaction of methylenetetrahydrofolate reductase from *Escherichia coli*. *Biochemistry* **2009**, *48*, 7673−7685.
(4) Estrada, A.; Wright, D. L.; Anderson, A. C. Antibacterial Antifolates: From Development through Resistance to the Next Generation. *Cold Spring Harb. Perspect. Med.* **2016**, *6* (8), No. a028324.
(5) Fernandez-Villa, D.; Aguilar, M. R.; Rojo, L. Folic Acid Antagonists: Antimicrobial and Immunomodulating Mechanisms and Applications. *Int. J. Mol. Sci.* **2019**, *20* (20), 4996.
(6) Nixon, M. R.; Saionz, K. W.; Koo, M. S.; Szymonifka, M. J.; Jung, H.; Roberts, J. P.; Nandakumar, M.; Kumar, A.; Liao, R.; Rustad, T.; Sacchettini, J. C.; Rhee, K. Y.; Freundlich, J. S.; Sherman, D. R. Folate pathway disruption leads to critical disruption of methionine derivatives in *Mycobacterium tuberculosis*. *Chem. Biol.* **2014**, *21*, 819−830.
(7) Sah, S.; Lahry, K.; Talwar, C.; Singh, S.; Varshney, U. Monomeric NADH-Oxidizing Methylenetetrahydrofolate Reductases from *Mycobacterium smegmatis* Lack Flavin Coenzyme. *J. Bacteriol.* **2020**, *202* (12), No. e00709-19, DOI: 10.1128/jb.00709-19.
(8) Trimmer, E. E.; Ballou, D. P.; Galloway, L. J.; Scannell, S. A.; Brinker, D. R.; Casas, K. R. Aspartate 120 of Escherichia coli methylenetetrahydrofolate reductase: evidence for major roles in folate binding and catalysis and a minor role in flavin reactivity. *Biochemistry* **2005**, *44*, 6809−6822.
(9) Zuo, C.; Jolly, A. L.; Nikolova, A. P.; Satzer, D. I.; Cao, S.; Sanchez, J. S.; Ballou, D. P.; Trimmer, E. E. A role for glutamine 183 in the folate oxidative half-reaction of methylenetetrahydrofolate reductase from *Escherichia coli*. *Arch. Biochem. Biophys.* **2018**, *642*, 63−74.
(10) Li, J.; Yang, M.; Li, W.; Lu, C.; Feng, D.; Shang, Z.; Wang, C.; Lin, W. Structural and Functional Characterization of a Mycobacterial Methylenetetrahydrofolate Reductase Utilizing NADH as the Exclusive Cofactor. *Biochem. J.* **2023**, *480* (14), 1129−1146.
(11) Guzzo, M. B.; Nguyen, H. T.; Pham, T. H.; Wyszczelska-Rokiel, M.; Jakubowski, H.; Wolff, K. A.; Ogwang, S.; Timpona, J. L.; Gogula, S.; Jacobs, M. R.; Ruetz, M.; Krautler, B.; Jacobsen, D. W.; Zhang, G. F.; Nguyen, L. Methylfolate Trap Promotes Bacterial Thymineless Death by Sulfa Drugs. *PLoS Pathog.* **2016**, *12* (10), No. e1005949.
(12) Ovung, A.; Bhattacharyya, J. Sulfonamide drugs: structure, antibacterial property, toxicity, and biophysical interactions. *Biophys. Rev.* **2021**, *13*, 259−272.
(13) He, S. C.; Ponmani, J.; Avula, S.; Zhang, H.-Z.; Wang, X.-L.; Zhou, C. H. Recent advance in sulfonamide-based medicinal chemistry. *Sci. Sin. Chim.* **2016**, *46*, 823−847.
(14) Sah, S.; Shah, R. A.; Govindan, A.; Varada, R.; Rex, K.; Varshney, U. Utilisation of 10-formyldihydrofolate as substrate by dihydrofolate reductase (DHFR) and 5-aminoimidazole-4-carboxamide ribonucleotide (AICAR) tranformylase/IMP cyclohydrolase (PurH) in *Escherichia coli*. *Microbiology* **2018**, *164*, 982−991.
(15) Schnell, J. R.; Dyson, H. J.; Wright, P. E. Structure, dynamics, and catalytic function of dihydrofolate reductase. *Annu. Rev. Biophys. Biomol. Struct.* **2004**, *33*, 119−140.
(16) Guenther, B. D.; Sheppard, C. A.; Tran, P.; Rozen, R.; Matthews, R. G.; Ludwig, M. L. The structure and properties of methylenetetrahydrofolate reductase from *Escherichia coli* suggest how folate ameliorates human hyperhomocysteinemia. *Nat. Struct. Biol.* **1999**, *6*, 359−365.
(17) Igari, S.; Ohtaki, A.; Yamanaka, Y.; Sato, Y.; Yohda, M.; Odaka, M.; Noguchi, K.; Yamada, K. Properties and crystal structure of methylenetetrahydrofolate reductase from *Thermus thermophilus* HB8. *PLoS One* **2011**, *6* (8), No. e23716.
(18) Pejchal, R.; Sargeant, R.; Ludwig, M. L. Structures of NADH and CH3-H4folate complexes of *Escherichia coli* methylenetetrahydrofolate reductase reveal a spartan strategy for a ping-pong reaction. *Biochemistry* **2005**, *44*, 11447−11457.
(19) Sheppard, C. A.; Trimmer, E. E.; Matthews, R. G. Purification and properties of NADH-dependent 5, 10-methylenetetrahydrofolate reductase (MetF) from *Escherichia coli*. *J. Bacteriol.* **1999**, *181*, 718−725.
(20) Trimmer, E. E.; Ballou, D. P.; Ludwig, M. L.; Matthews, R. G. Folate activation and catalysis in methylenetetrahydrofolate reductase from *Escherichia coli*: roles for aspartate 120 and glutamate 28. *Biochemistry* **2001**, *40*, 6216−6226.
(21) Trimmer, E. E.; Ballou, D. P.; Matthews, R. G. Methylenetetrahydrofolate reductase from *Escherichia coli*: elucidation of the kinetic mechanism by steady-state and rapid-reaction studies. *Biochemistry* **2001**, *40*, 6205−6215.
(22) Froese, D. S.; Kopec, J.; Rembeza, E.; Bezerra, G. A.; Oberholzer, A. E.; Suormala, T.; Lutz, S.; Chalk, R.; Borkowska, O.; Baumgartner, M. R.; Yue, W. W. Structural basis for the regulation of human 5,10-methylenetetrahydrofolate reductase by phosphorylation

and S-adenosylmethionine inhibition. *Nat. Commun.* **2018**, *9*, 2261 DOI: 10.1038/s41467-018-04735-2.
(23) Bertsch, J.; Oppinger, C.; Hess, V.; Langer, J. D.; Muller, V. Heterotrimeric NADH-oxidizing methylenetetrahydrofolate reductase from the acetogenic bacterium *Acetobacterium woodii*. *J. Bacteriol.* **2015**, *197*, 1681−1689.
(24) Matthews, R. G. Methylenetetrahydrofolate reductase from pig liver. *Methods Enzymol.* **1986**, *122*, 372−381.
(25) Sun, D. F.; Weng, Y. R.; Chen, Y. X.; Lu, R.; Wang, X.; Fang, J. Y. Knock-down of methylenetetrahydrofolate reductase reduces gastric cancer cell survival: an *in vitro* study. *Cell Biol. Int.* **2008**, *32*, 879−887.
(26) Yamada, K.; Strahler, J. R.; Andrews, P. C.; Matthews, R. G. Regulation of human methylenetetrahydrofolate reductase by phosphorylation. *Proc. Natl. Acad. Sci. U. S. A.* **2005**, *102*, 10454−10459.
(27) Yu, J. F.; Xu, J. T.; Yang, S. S.; Gao, M. N.; Si, H. R.; Xiong, D. Y.; Gu, J.; Wu, Z. L.; Zhou, J.; Deng, J. Y. Decreased Methylenetetrahydrofolate Reductase Activity Leads to Increased Sensitivity to *para*-Aminosalicylic Acid in *Mycobacterium tuberculosis*. *Antimicrob. Agents Chemother.* **2022**, *66* (1), No. e0146521, DOI: 10.1128/AAC.01465-21.
(28) Tan, W.; Liao, T. H.; Wang, J.; Ye, Y.; Wei, Y. C.; Zhou, H. K.; Xiao, Y.; Zhi, X. Y.; Shao, Z. H.; Lyu, L. D.; Zhao, G. P. A recently evolved diflavin-containing monomeric nitrate reductase is responsible for highly efficient bacterial nitrate assimilation. *J. Biol. Chem.* **2020**, *295*, 5051−5066.
(29) Burda, P.; Schafer, A.; Suormala, T.; Rummel, T.; Burer, C.; Heuberger, D.; Frapolli, M.; Giunta, C.; Sokolova, J.; Vlaskova, H.; Kozich, V.; Koch, H. G.; Fowler, B.; Froese, D. S.; Baumgartner, M. R. Insights into Severe 5,10-Methylenetetrahydrofolate Reductase Deficiency: Molecular Genetic and Enzymatic Characterization of 76 Patients. *Hum. Mutat.* **2015**, *36*, 611−621.
(30) Burda, P.; Suormala, T.; Heuberger, D.; Schafer, A.; Fowler, B.; Froese, D. S.; Baumgartner, M. R. Functional characterization of missense mutations in severe methylenetetrahydrofolate reductase deficiency using a human expression system. *J. Inherited Metab. Dis.* **2017**, *40*, 297−306.
(31) Morris, G. M.; Huey, R.; Lindstrom, W.; Sanner, M. F.; Belew, R. K.; Goodsell, D. S.; Olson, A. J. AutoDock4 and AutoDockTools4: Automated docking with selective receptor flexibility. *J. Comput. Chem.* **2009**, *30*, 2785−2791.
(32) White, R. L.; Burgess, D. S.; Manduru, M.; Bosso, J. A. Comparison of three different in vitro methods of detecting synergy: time-kill, checkerboard, and E test. *Antimicrob. Agents Chemother.* **1996**, *40*, 1914−1918.
(33) Meletiadis, J.; Pournaras, S.; Roilides, E.; Walsh, T. J. Defining fractional inhibitory concentration index cutoffs for additive interactions based on self-drug additive combinations, Monte Carlo simulation analysis, and in vitro-in vivo correlation data for antifungal drug combinations against Aspergillus fumigatus. *Antimicrob. Agents Chemother.* **2010**, *54*, 602−609.
(34) Lin, Z.; Sun, Y.; Liu, Y.; Tong, S.; Shang, Z.; Cai, Y.; Lin, W. Structural and Functional Analyses of the Transcription Repressor DgoR From *Escherichia coli* Reveal a Divalent Metal-Containing D-Galactonate Binding Pocket. *Front. Microbiol.* **2020**, *11*, No. 590330.

https://doi.org/10.1021/acsomega.3c05021
ACS Omega 2023, 8, 38406−38417